AD-A031 907

AD A031907

AD

Report 2179

SPALLATION RESULTING FROM HIGH-VELOCITY IMPACTS

May 1976

U.S. ARMY MOBILITY EQUIPMENT
RESEARCH AND DEVELOPMENT COMMAND
FORT BELVOIR, VIRGINIA

REPORT DOCUMENTATION PAGE

READ INSTRUCTIONS BEFORE COMPLETING FORM

1. REPORT NUMBER 2179	2. GOVT ACCESSION NO.	3. RECIPIENT'S CATALOG NUMBER
4. TITLE (and Subtitle) SPALLATION RESULTING FROM HIGH-VELOCITY IMPACTS		5. TYPE OF REPORT & PERIOD COVERED Final; June 1974 through April 1975 6. PERFORMING ORG. REPORT NUMBER
7. AUTHOR(s) Dr. Ray Kinslow		8. CONTRACT OR GRANT NUMBER(s)
9. PERFORMING ORGANIZATION NAME AND ADDRESS U.S. Army Mobility Equipment Research and Development Command, ATTN: DRXFB-XS Fort Belvoir, Virginia 22060		10. PROGRAM ELEMENT, PROJECT, TASK AREA & WORK UNIT NUMBERS Project 1K161101A91A
11. CONTROLLING OFFICE NAME AND ADDRESS U.S. Army Mobility Equipment Research and Development Command Fort Belvoir, Virginia 22060		12. REPORT DATE May 1976 13. NUMBER OF PAGES 42
14. MONITORING AGENCY NAME & ADDRESS(if different from Controlling Office)		15. SECURITY CLASS. (of this report) Unclassified 15a. DECLASSIFICATION/DOWNGRADING SCHEDULE

16. DISTRIBUTION STATEMENT (of this Report)

Approved for public release; distribution unlimited.

17. DISTRIBUTION STATEMENT (of the abstract entered in Block 20, if different from Report)

18. SUPPLEMENTARY NOTES

19. KEY WORDS (Continue on reverse side if necessary and identify by block number)

Fracture
Hypervelocity Impact
Spallation

20. ABSTRACT (Continue on reverse side if necessary and identify by block number)

A high-velocity impact generally creates a crater in the structure, driving a strong shock wave into it. If the impacted structure, or target, is sufficiently thin, a puncture will result. If the target is relatively thick, the shock will rapidly decay into an elastic stress wave. When such a wave encounters a free surface, it is reflected, generally as a tensile wave, and its amplitude may be of sufficient magnitude to produce fractures near the surface. Such fractures may appear as granular cracks, as rear surface bulges, or as a complete detachment of target material, creating a shrapnel effect. An analysis of these phenomena is presented herein.

CONTENTS

Paragraph	Title	Page
	Illustrations	iv
1	Introduction	1
2	Mechanism of Spallation	1
3	Spall Location and Velocity	1
4	Numerical Examples	8
5	Experimental Determination of Free-Surface Velocity	10
6	Conclusion	28

ILLUSTRATIONS

Figure	Title	Page
1	Fractures Produced by Reflected Stress Waves	2
2	Mechanics of Spall	3
3	Spall Location and Velocity	5
4	Spall Velocity for Armor Steel	9
5	Fracture Locations in Armor Steel	10
6	Stress Waves in Semi-Infinite Target	12
7	Reflected Stress Waves for t-values of 80 to 100	13
8	Reflected Stress Waves for t-values of 80 to 90	14
9	Maximum Tensile Stress for x-values of 0 to 1.5	15
10	Maximum Tensile Stress for x-values of 2.0 to 3.5	16
11	Location and Extent of Fractures	17
12	Maximum Principal Stress (p) for t-values of 80, 85, and 90	18
13	Maximum Principal Stress (p) for t-values of 95 and 100	19
14	Minimum Principal Stress (q) for t-values of 80, 85, and 90	20
15	Minimum Principal Stress (q) for t-values of 95 and 100	21
16	Maximum Shear Stress (p - q) for t-values of 80, 85, and 90	22
17	Maximum Shear Stress (p - q) for t-values of 95 and 100	23
18	Deformation of Rear Surface	24
19	Displacement of Rear Surface as a Function of Time	25
20	Initial Surface Velocities at Various Locations	26
21	Front Surface Cratering and Rear Surface Fractures	27

SPALLATION RESULTING FROM HIGH-VELOCITY IMPACTS

1. **Introduction.** A high-velocity impact generally creates a crater in a structure, driving a strong shock wave into it. If the impacted structure, or target, is sufficiently thin, a puncture will result. If the target is relatively thick, the shock will rapidly decay into an elastic stress wave. When such a wave encounters a free surface, it is reflected, generally as a tensile wave, and its amplitude may be of sufficient magnitude to produce fractures near the surface. Such fractures may appear as granular cracks, as rear surface bulges, or as a complete detachment of target material, creating a shrapnel effect. An example of each of these is shown in Figure 1 for copper, aluminum, and steel targets.

2. **Mechanism of Spallation.** The mechanism of fracture caused by the reflection of a pressure wave from a free surface is illustrated in Figure 2. In this example, a sawtooth wave profile is assumed for both the simplicity of the calculations and because it is probably a fair approximation of the average pressure wave. It is assumed that this pulse has a length λ and a maximum amplitude of σ_o, which is greater than the critical tensile strength σ_o of the material. The resultant stress at any point during reflection is obtained by adding the stresses caused by the incident and reflected waves. At (a) the pulse has just reached the rear surface of the target. At (b), a short time later, some tensile stress is seen near the boundary. This tension increases in magnitude until it reaches the critical fracture strength of the material σ_c, as shown in (c). When the tensile stress reaches this critical value, a fracture will be formed approximately parallel to the rear surface. This fracture acts as a new free surface from which the tail of the pressure pulse is reflected. The tensile stress produced by the reflection increases as shown in (d) and may again reach the critical value, at which time a second fracture, shown at (e), will be formed parallel to the first. The tail of the pulse is now reflected from this newly formed free surface and, if of sufficient magnitude, will produce additional fractures.

3. **Spall Location and Velocity.** From the geometry of the pulse, it may be seen that if there is a fracture it will be located at a distance

$$\Delta = \frac{\sigma_c}{\sigma_o} \frac{\lambda}{2} \tag{1}$$

from the rear surface. In this case of the sawtooth pulse, if other fractures are formed, they also will be the distance Δ apart.

A portion of the wave is trapped in the material between the rear surface and the first fracture. The free-surface velocity V_s can be found by equating the impulse of

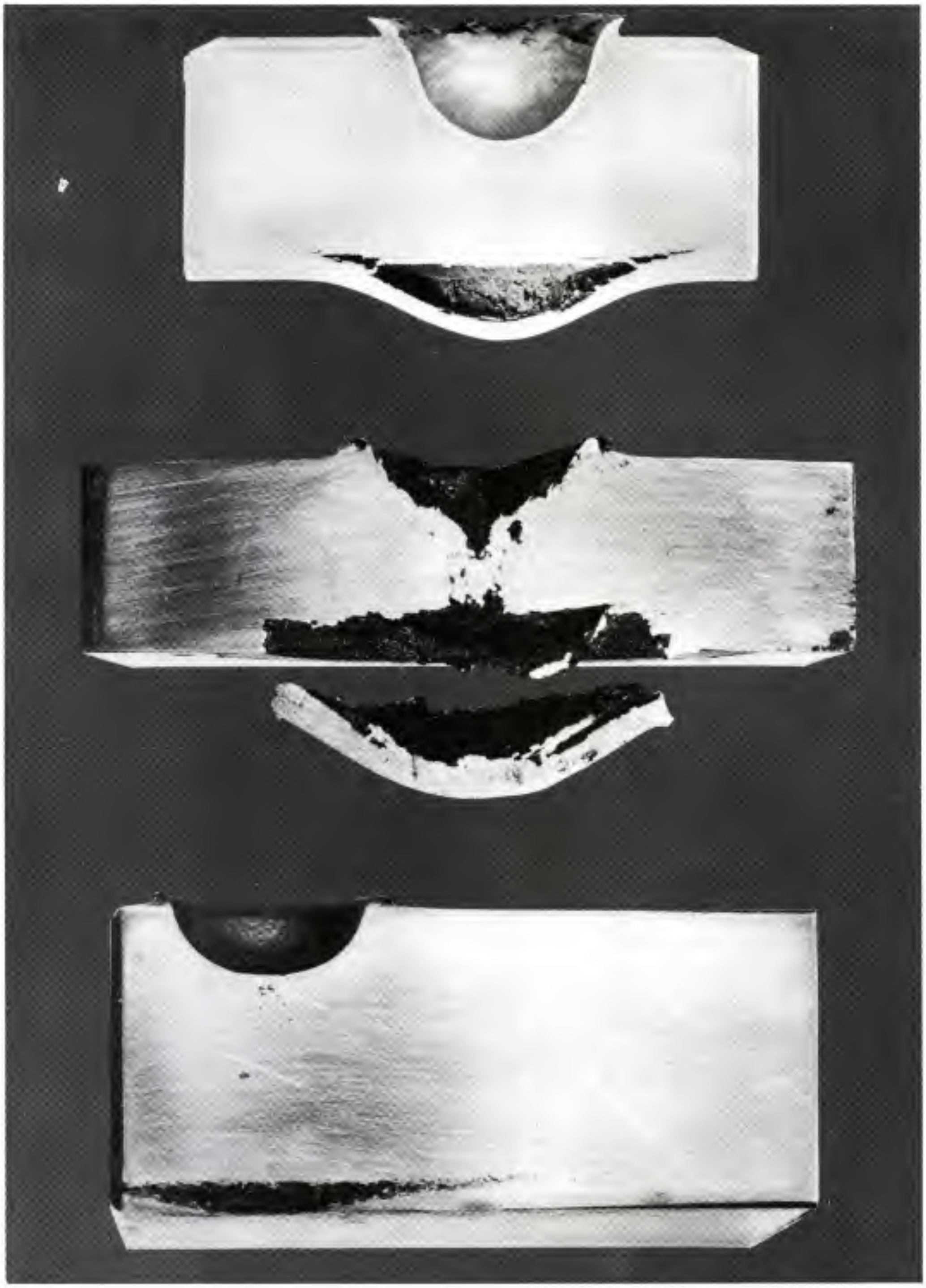

Figure 1. Fractures produced by reflected stress waves.

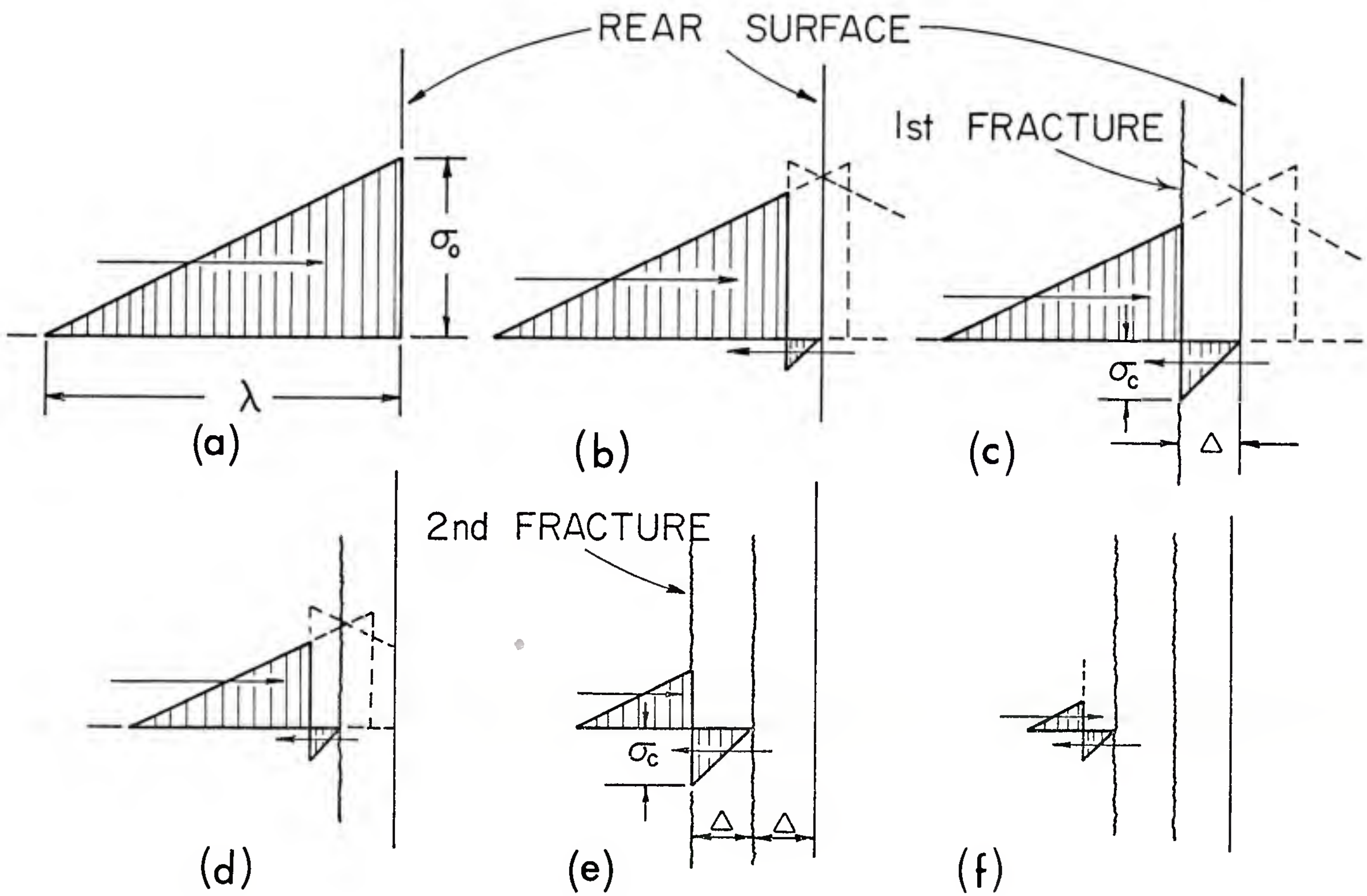

Figure 2. Mechanics of spall.

the trapped part of the wave to the momentum of that portion of the material:

$$\rho \Delta V_s = \frac{\sigma_o + (\sigma_o - \sigma_c)}{2} \, t, \tag{2}$$

where ρ is the material density, and t is $2\Delta/c$, the time since the pulse front passed the point of fracture (c = pulse velocity). The portion of material between the fracture and the rear surface is known as the "spall," and the separation of the fractured material from the original material is called "spallation."

The material velocity located in the spall is, therefore:

$$V_s = \frac{2\sigma_o - \sigma_c}{\rho c} \, . \tag{3}$$

The initial velocity of the spall center can be approximated by this material velocity and will be referred to as the spall velocity.

Equating the impulse of the portion of the pulse trapped between the first and second fractures to its momentum gives the velocity of the second spall:

$$V_{s2} = \frac{(\sigma_o - \sigma_c) + (\sigma_o - 2\sigma_c)}{2} \, ,$$

$$= \frac{2\sigma_o - 3\sigma_c}{\rho c} \, . \tag{4}$$

If the pulse amplitude is sufficiently great to produce a third fracture, the velocity of the material between the second and third fractures will be:

$$V_{s3} = \frac{2\sigma_o - 5\sigma_c}{\rho c} \, . \tag{5}$$

The maximum possible number of spalls n will be σ_o/σ_c.

The velocity of any spall can be given by the relation:

$$V_{sn} = \frac{2\sigma_o - (2n - 1)\,\sigma_c}{\rho c} \, . \tag{6}$$

Next, a more general pulse having a trapezoidal profile as shown in Figure 3, Part A, is considered. Since the rise time is usually less than the decay time, only the

	Δ	V_S
A 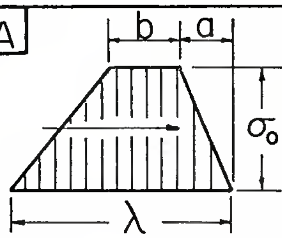	$\frac{(\lambda-a-b)}{2}\frac{\sigma_c}{\sigma_0}+\frac{b}{2}$	$\frac{2\sigma_0-\sigma_c}{\rho c}+\frac{b\sigma_c}{2\Delta\rho c}$
B $a=o$ 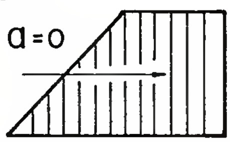	$\frac{(\lambda-b)}{2}\frac{\sigma_c}{\sigma_0}+\frac{b}{2}$	$\frac{2\sigma_0-\sigma_c}{\rho c}+\frac{b\sigma_c}{2\Delta\rho c}$
C $b=o$ 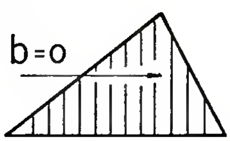	$\frac{(\lambda-a)}{2}\frac{\sigma_c}{\sigma_0}$	$\frac{2\sigma_0-\sigma_c}{\rho c}$
D $a=b=o$ 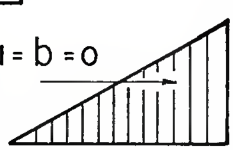	$\frac{\lambda}{2}\frac{\sigma_c}{\sigma_0}$	$\frac{2\sigma_0-\sigma_c}{\rho c}$
E $a=o,\ b=\lambda$ 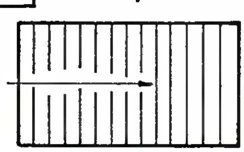	$\frac{\lambda}{2}$	$\frac{2\sigma_0}{\rho c}$
F $\sigma=\sigma_0 e^{-\alpha t}$ 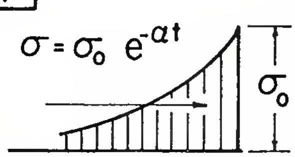	$-\frac{c}{2\alpha}\ln\left(1-\frac{\sigma_c}{\sigma_0}\right)$	$\frac{2\sigma_c}{\rho c\ \ln\left(1-\frac{\sigma_c}{\sigma_0}\right)}$

Figure 3. Spall location and velocity.

case when $a < (\lambda\text{-}a\text{-}b)$ will be considered. Also, only the first fracture causes significant spallation and the maximum material velocities; the possible additional fractures will not be considered.

From the geometry of this pulse, the fracture distance from the rear surface is found to be:

$$\Delta = \frac{(\lambda\text{-}a\text{-}b)}{2}\,\frac{\sigma_c}{\sigma_o} + \frac{b}{2}\,. \tag{7}$$

Equating the impulse for that portion of the pulse between the fracture and the surface to the material momentum gives:

$$V_s = \frac{b\sigma_o}{\Delta\rho c} + \frac{(2\Delta\text{-}b)\,(2\sigma_o - \sigma_c)}{2\Delta\rho c}\,,$$

$$= \frac{2\sigma_o - \sigma_c}{\rho c} + \frac{b\sigma_c}{2\Delta\rho c}\,. \tag{8}$$

These relations can be applied to any trapezoidal or triangular pulse as long as the rise time is less than the decay time. For example, the fracture location and material velocity for the sawtooth pulse previously considered could have been found by equations (7) and (8) when $a = b = 0$.

Equations for the spall thickness Δ and velocity V_s for various trapezoidal (and triangular) pulse profiles are also shown in Figure 3. From these relations, the following conclusions can be drawn:

a. If the pulse profile can be approximated by a triangle, neither the rise time a/c, nor the pulse length λ, nor the spall thickness Δ has any effect on the material velocity. The material characteristic impedance ρc, the pulse amplitude σ_o, and the material resistance to tensile stresses σ_c determine the spall velocity.

b. The spall thickness produced by a triangular pulse is affected by the pulse length and rise time as well as by the ratio of critical strength to pulse amplitude.

c. If the maximum pulse amplitude σ_o is exerted for a period of time b/c, both spall thickness Δ and velocity V_s will be affected. The thickness of the spall will be increased by $\left(1 - \frac{\sigma_c}{\sigma_o}\right)\frac{b}{2}$, and its velocity will be increased by $\frac{b\sigma_c}{2\Delta\rho c}$.

d. An increase in the rise time of either a triangular or trapezoidal pulse

decreases the spall thickness by the amount of $\frac{a\,\sigma_c}{2\,\sigma_o}$.

e. In the case of a step function or rectangular pulse, the spall thickness will simply be $\lambda/2$, and the material velocity will be $2\sigma_o/\rho c$. Neither the spall location nor velocity depends upon the material strength as long as $\sigma_o > \sigma_c$. This is the relation generally used to determine the free-surface velocity, but it applies only when this pulse shape is assumed.

Another waveform will be considered before numerical values are calculated. The decaying exponential pulse $p = p_o e^{-\alpha t}$, where p_o is the initial pressure pulse and α is the decay constant, often has been used to represent the wave resulting from impact. It can be shown that the spall thickness resulting from the reflection of this wave from a free surface is:

$$\Delta = -\frac{c}{2\alpha}\,\ell n\left(1 - \frac{\sigma_c}{\sigma_o}\right) . \tag{9}$$

The material velocity is given by the relations,

$$V_s = \frac{\sigma_o \left(e^{\frac{-2\alpha\Delta}{c}}\right) - 1}{\Delta\alpha\rho} , \tag{10}$$

$$= \frac{-2\sigma_c}{\rho c\,\ell n\left(1 - \frac{\sigma_c}{\sigma_o}\right)} \text{, and} \tag{11}$$

$$= \frac{\sigma_c}{\rho\alpha\Delta} . \tag{12}$$

A comparison of the spall velocity resulting from a triangular pulse as given by equation (3),

$$V_s = \frac{2\sigma_o - \sigma_c}{\rho c} ,$$

and that caused by an exponential pulse as given by equation (11),

$$V_s = \frac{2\sigma_c}{\rho c\,\ell n\left(1 - \frac{\sigma_c}{\sigma_o}\right)} ,$$

shows that both involve the same variables: ρ, c, σ_c, and σ_o.

4. **Numerical Examples.** In order to determine the spallation of armor steel the following material properties are assumed:

$$\sigma_c = 38 \text{ kb} = 5.51 \times 10^5 \text{ psi}$$
$$\rho = 7.33 \times 10^8 \text{ lb } (\mu\text{sec})^2/\text{in}^4$$
$$c = 0.234 \text{ in}/\mu\text{sec}$$

Material velocities resulting from both a triangular and an exponential pulse have been computed. Both sets of values are given in the table. These data are shown in graphical form in Figure 4. Except for the higher σ_c/σ_o ratios, there is little difference between the two.

Comparison of Material Velocities Resulting from Triangular and Exponential Pressure Pulses

	σ_o		V_s (ft/sec)		Ratio of Velocities
σ_c/σ_o	$(10)^5$ psi	kb	Triangular	Exponential	(Exp./Tri.)
0.2	27.5	190.0	2,404	2,400	0.998
0.3	18.4	126.7	1,520	1,501	0.988
0.4	13.8	95.0	1,073	1,048	0.977
0.5	11.0	76.0	801	772	0.964
0.6	9.18	63.3	624	584	0.936
0.7	7.87	54.3	497	445	0.895
0.8	6.89	47.5	402	333	0.828
0.9	6.12	42.2	327	233	0.713
0.95	5.80	40.0	296	179	0.605

Although there is little difference between the spall velocities resulting from the triangular and the exponential stress waves, there are large differences in the spall thickness resulting from the two. In both cases, the spall thickness Δ is a function of σ_c/σ_o. In the case of a triangular pulse, its length λ is an important parameter; whereas, the ratio of pulse velocity to the decay constant c/α is significant in the case of the exponential pulse. The dependence of the spall thickness upon the decay constant is shown in Figure 5. These relations are linear in the case of triangular pulses of various lengths.

The examples that have been given for very simple pulse forms are, of course, not too realistic, but they do enable one to determine the parameters that affect the spallation of a target.

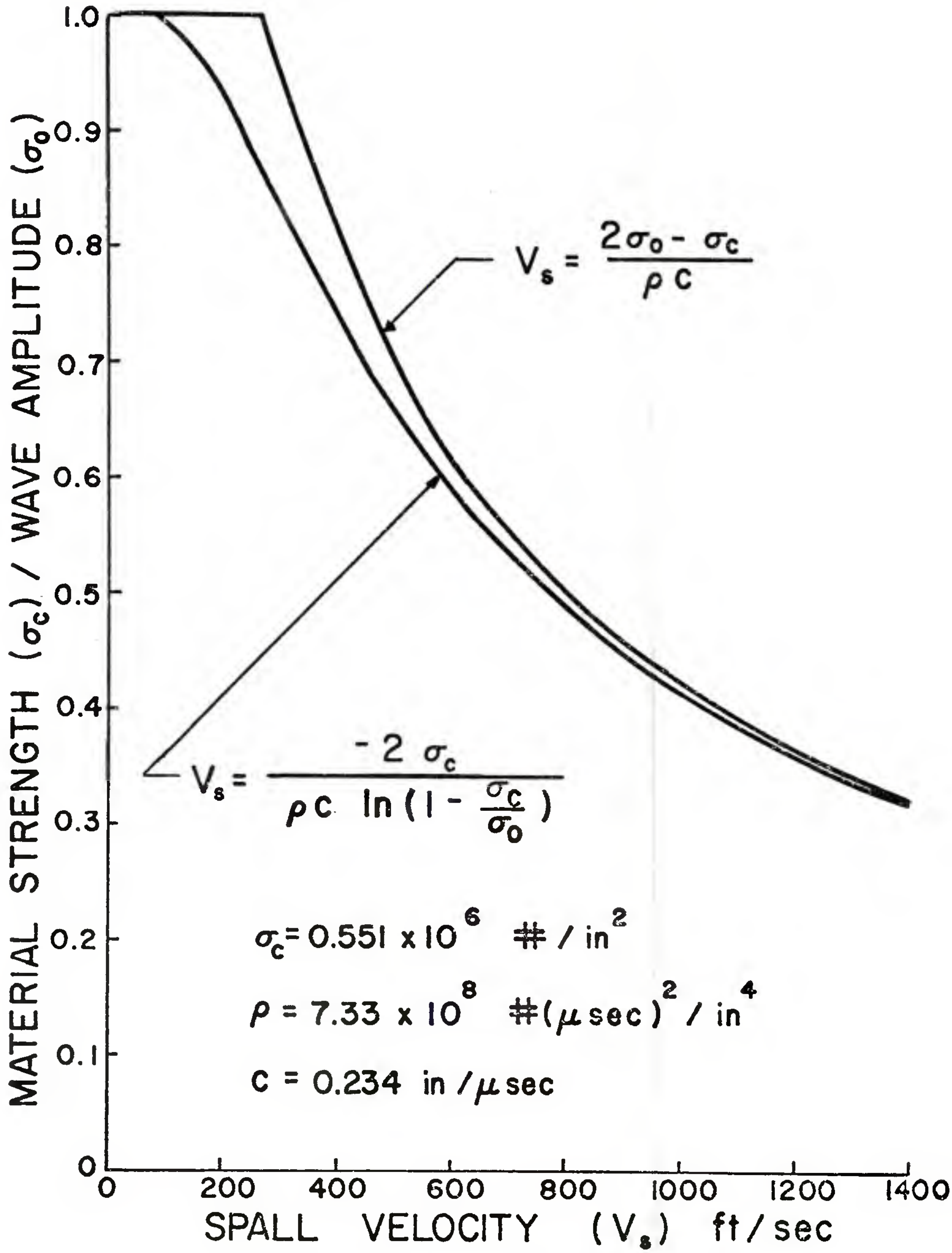

Figure 4. Spall velocity for armor steel.

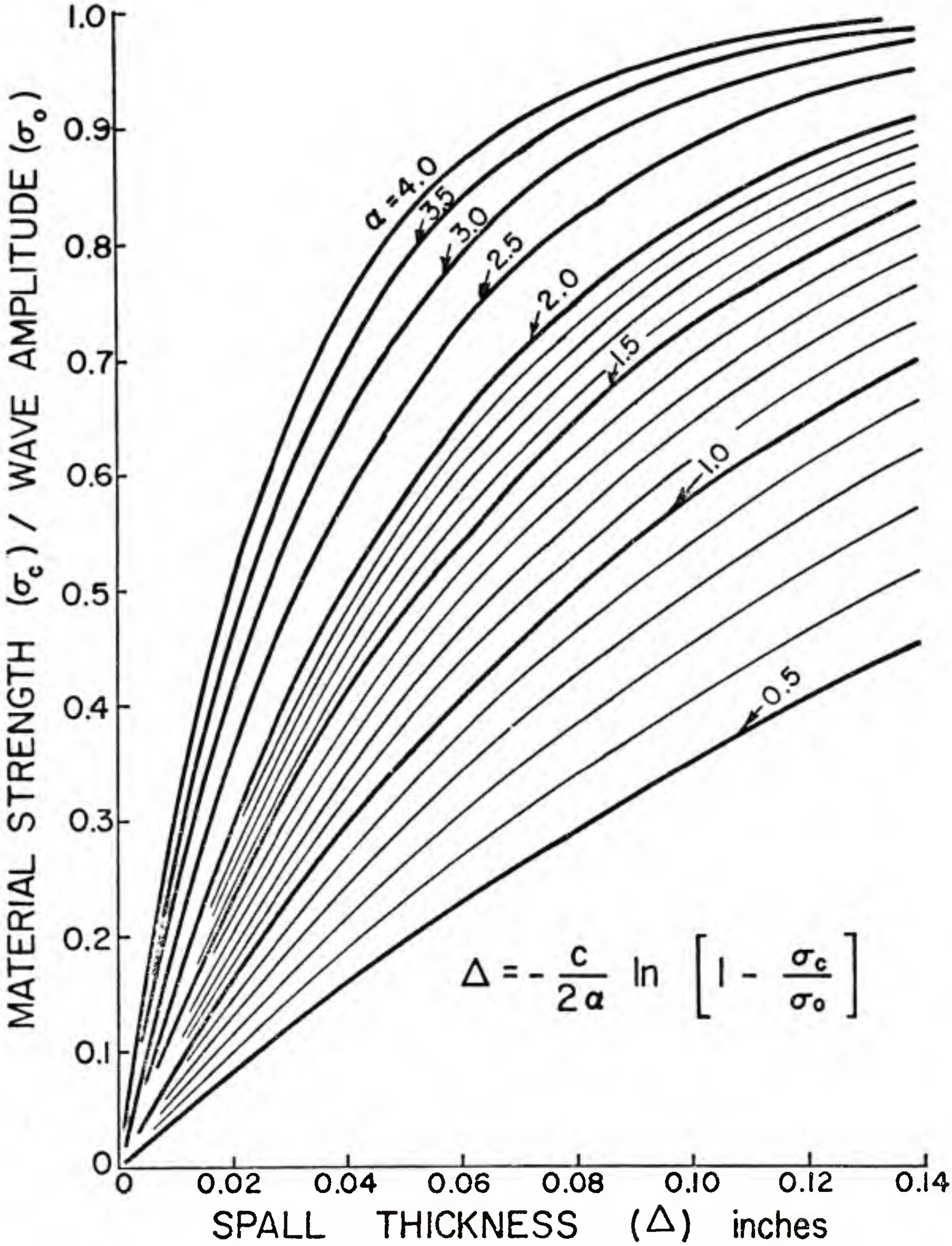

Figure 5. Fracture locations in armor steel.

A better representation of actual stress waves moving through a semi-infinite target is given in Figure 6. These are spherical stress waves resulting from an initial pressure pulse described by the relation:

$$p_o = (10)^4 \; [\exp(-0.001t) - \exp(-0.010t)].$$

These are relative values only.

Figures 7 and 8 show these waves as they are reflected from a target having a thickness of 5 units. Figure 8 shows the development of the tensile stresses better since they were computed and plotted for smaller units of time. It should be noted that the reflected tensile wave combines with the tensile tail of the pressure pulse producing a tensile stress that may be of greater magnitude than the amplitude of the pressure wave. The maximum tensile stresses at various times and at different distances from the axis of symmetry are shown in Figures 9 and 10. From these curves, the extent of probable fracture for various values of σ_c/σ_o can be determined as shown in Figure 11. The solid lines show the fracture locations in materials such as steel or aluminum where a simple crack would form. The dotted lines enclose the areas where the stress exceeded the critical tensile strength and would be the extent of damage in materials such as Lucite or Plexiglas. The curve on this figure is a plot of spall thickness on the axis as a function of σ_c/σ_o and is seen to be similar to those shown on Figure 5. Contours showing the maximum principal, minium principal, and maximum shear stresses are given in Figures 12, 13, 14, 15, 16, and 17. The reflected transverse, or shear, waves as well as the reflected longitudinal waves were taken into account in the computation of these stresses.

5. **Experimental Determination of Free-Surface Velocity.** Figure 18 shows the deformation of the rear surface of a 1.5-inch aluminum target resulting from a 0.3- by 0.3-inch Lexan projectile impact having a velocity of 24,000 ft/s. The photographs also show minute particles being knocked from the rear surface. The surface and particle displacements at the center of the spall are shown in Figure 19. The slope of the surface-displacement curve represents the free-surface velocity. The slope of the particle-displacement curve, which is a straight line, gives the initial surface velocity more accurately than can be determined from the slope of the target surface curve. The initial velocity of the spall center was 1,120 ft/s. The surface velocities at various distances from the center are shown on Figure 20. This would be an excellent method for determining the surface velocity of armor steel for various impact conditions.

The reason for the erratic motion of the target surface is not known. Figure 21 shows this target after being sectioned and polished. It can be seen that multiple fractures were formed. It may be that the formation and movement of these additional spalls caused the movement of the rear surface after it had come to rest. It is difficult, however, to reconcile the times involved.

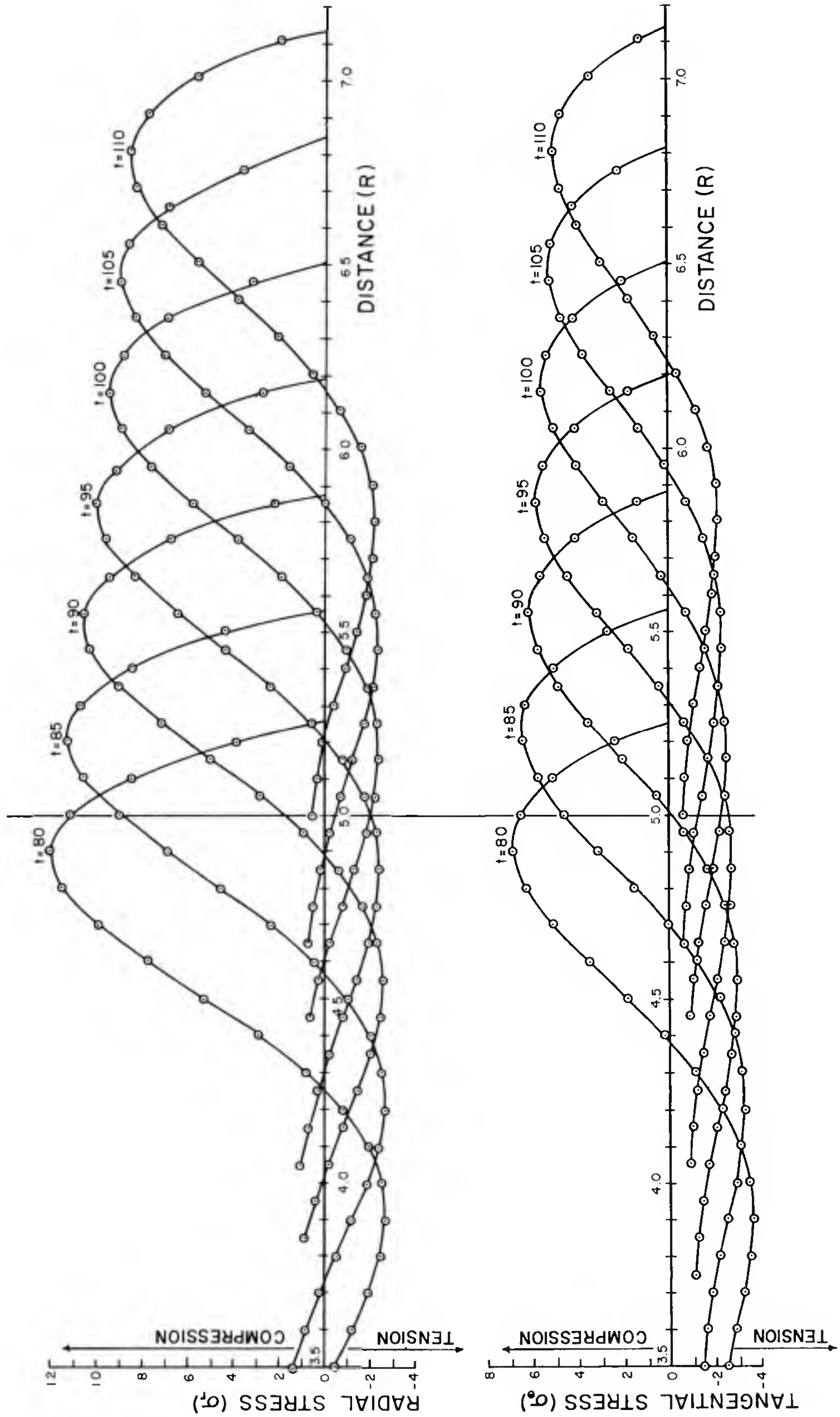

Figure 6. Stress waves in semi-infinite target.

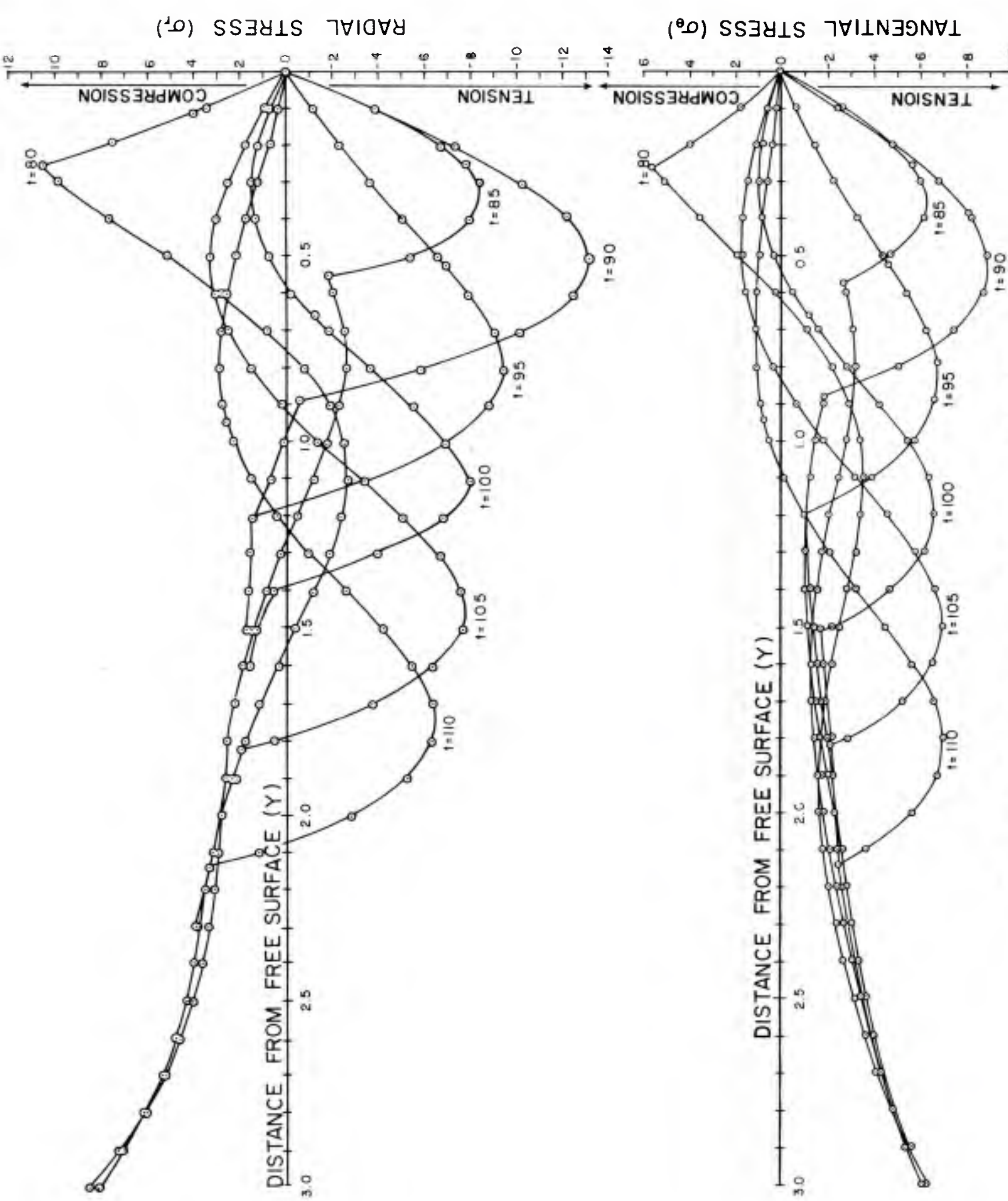

Figure 7. Reflected stress waves for t-values of 80 to 110.

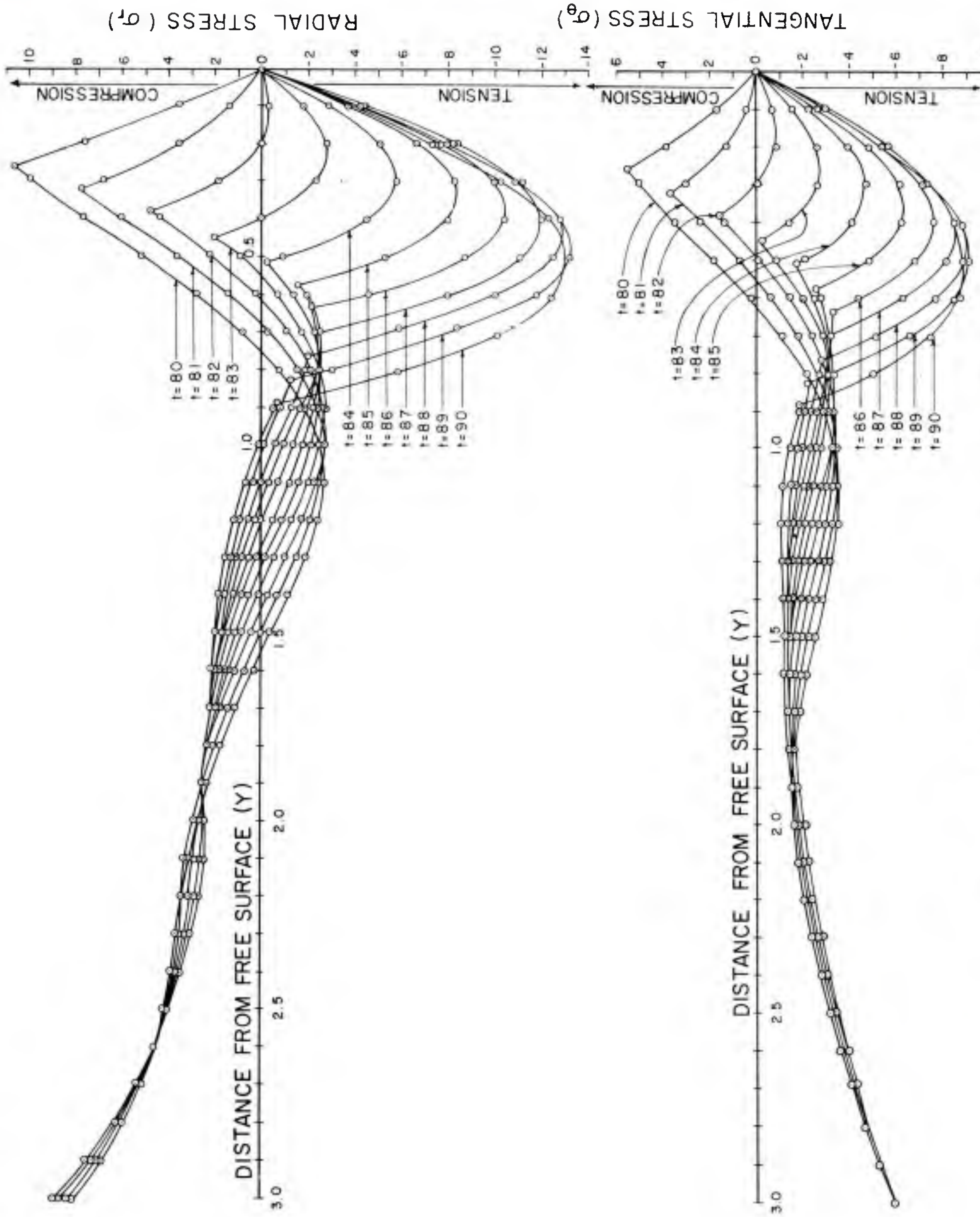

Figure 8. Reflected stress waves for t-values of 80 to 90.

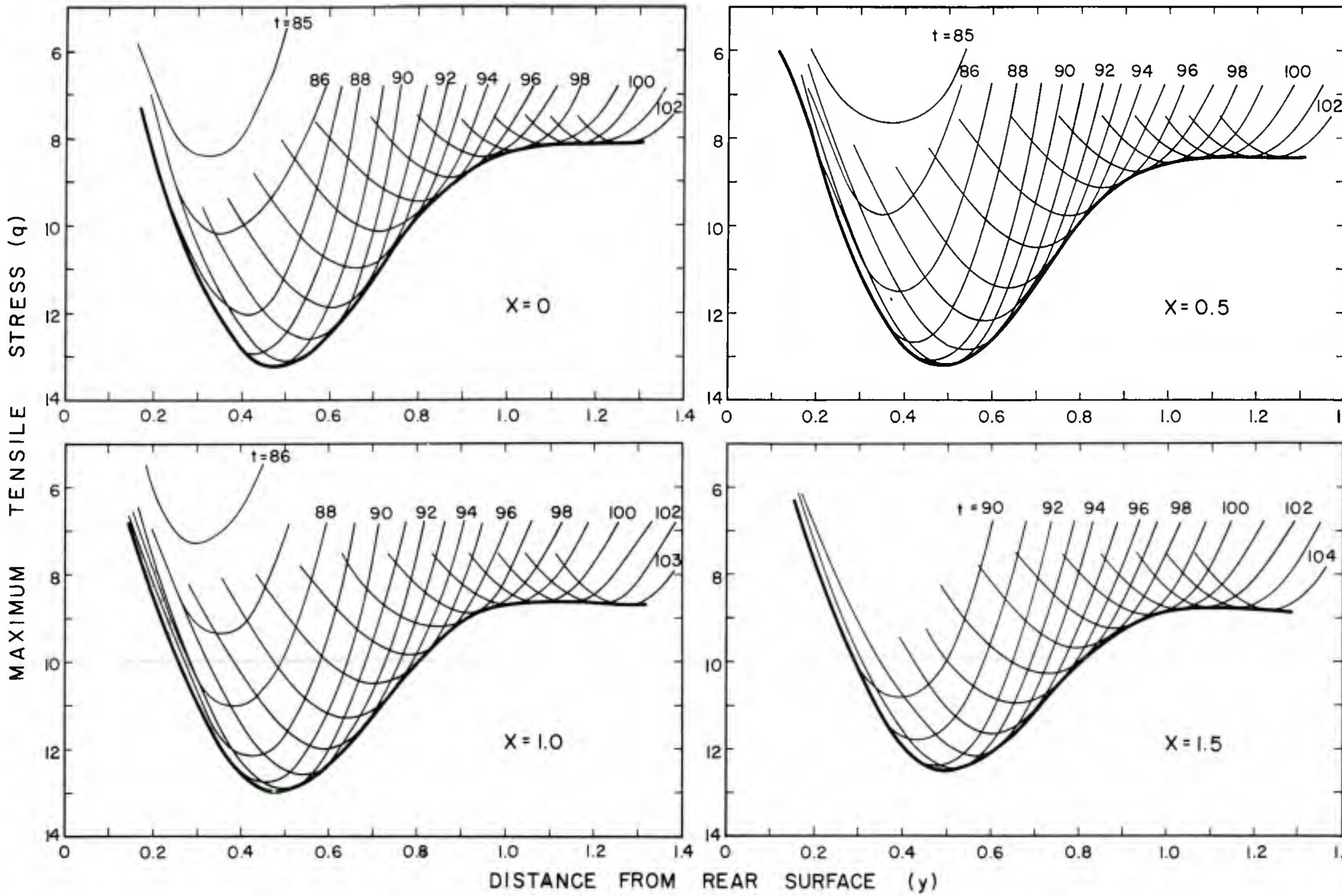

Figure 9. Maximum tensile stress for x-values of 0 to 1.5.

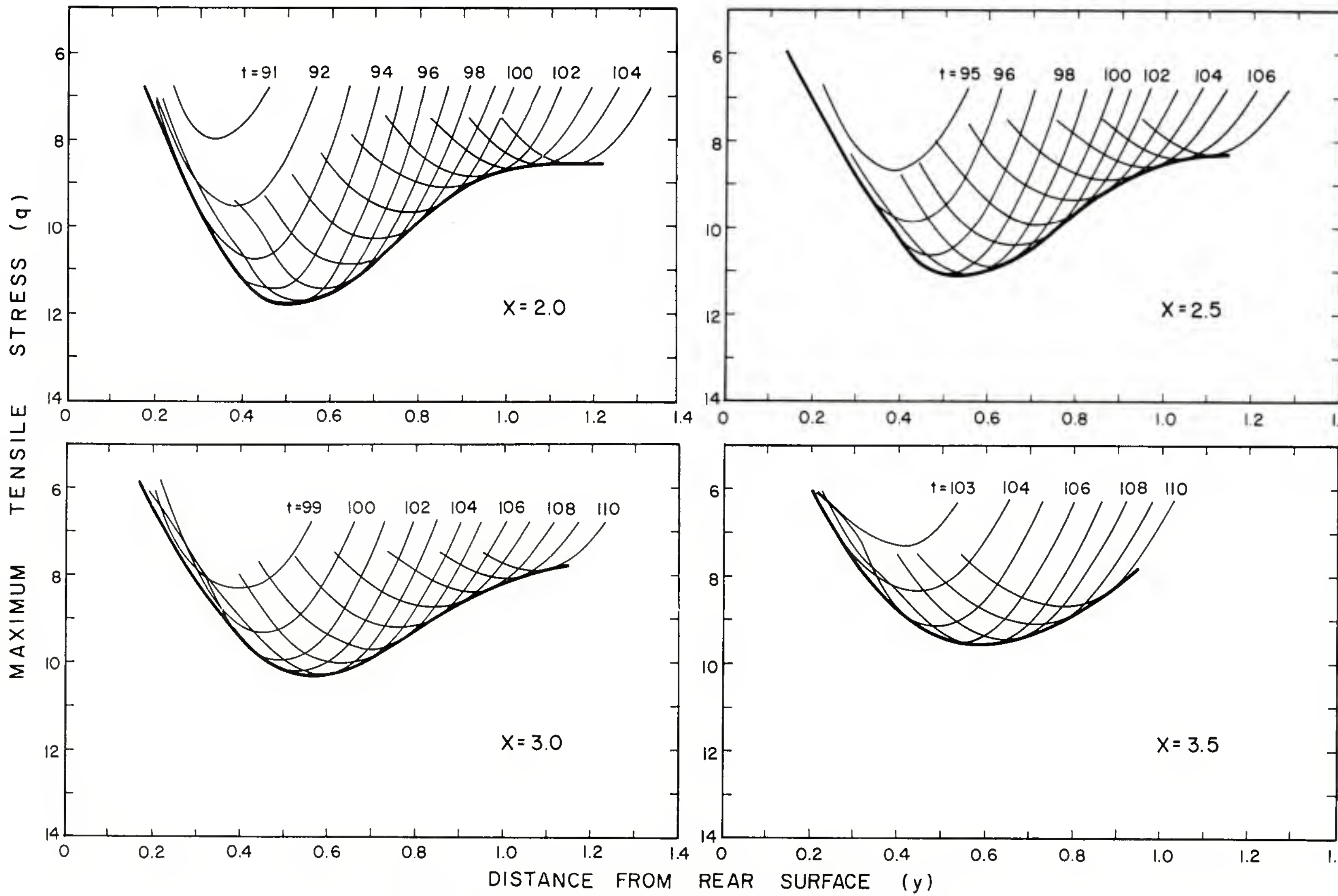

Figure 10. Maximum tensile stress for x-values of 2.0 to 3.5.

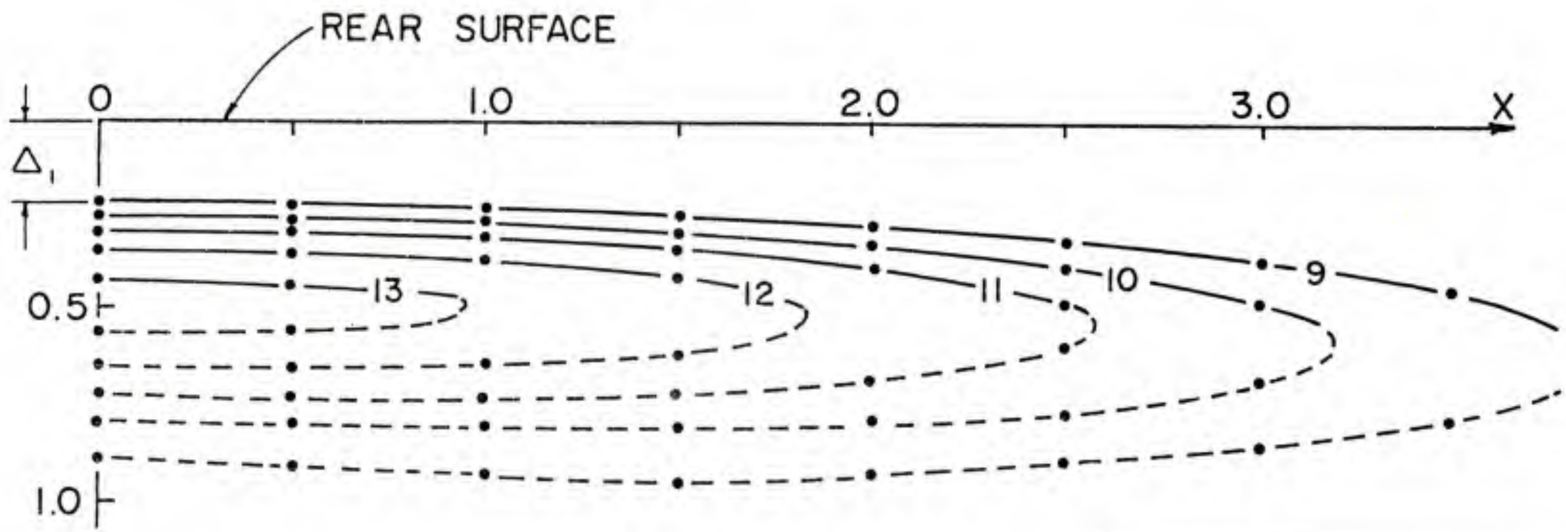

Relative Value of Stress	σ_c/σ_o	Fracture Location Δ
9	0.75	0.21
10	0.83	0.24
11	0.92	0.28
12	1.00	0.33
13	1.08	0.41

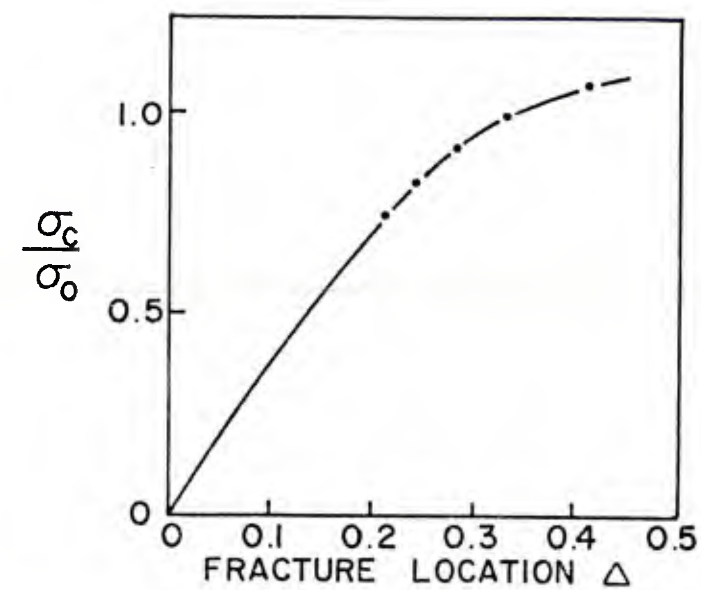

Figure 11. Location and extent of fractures.

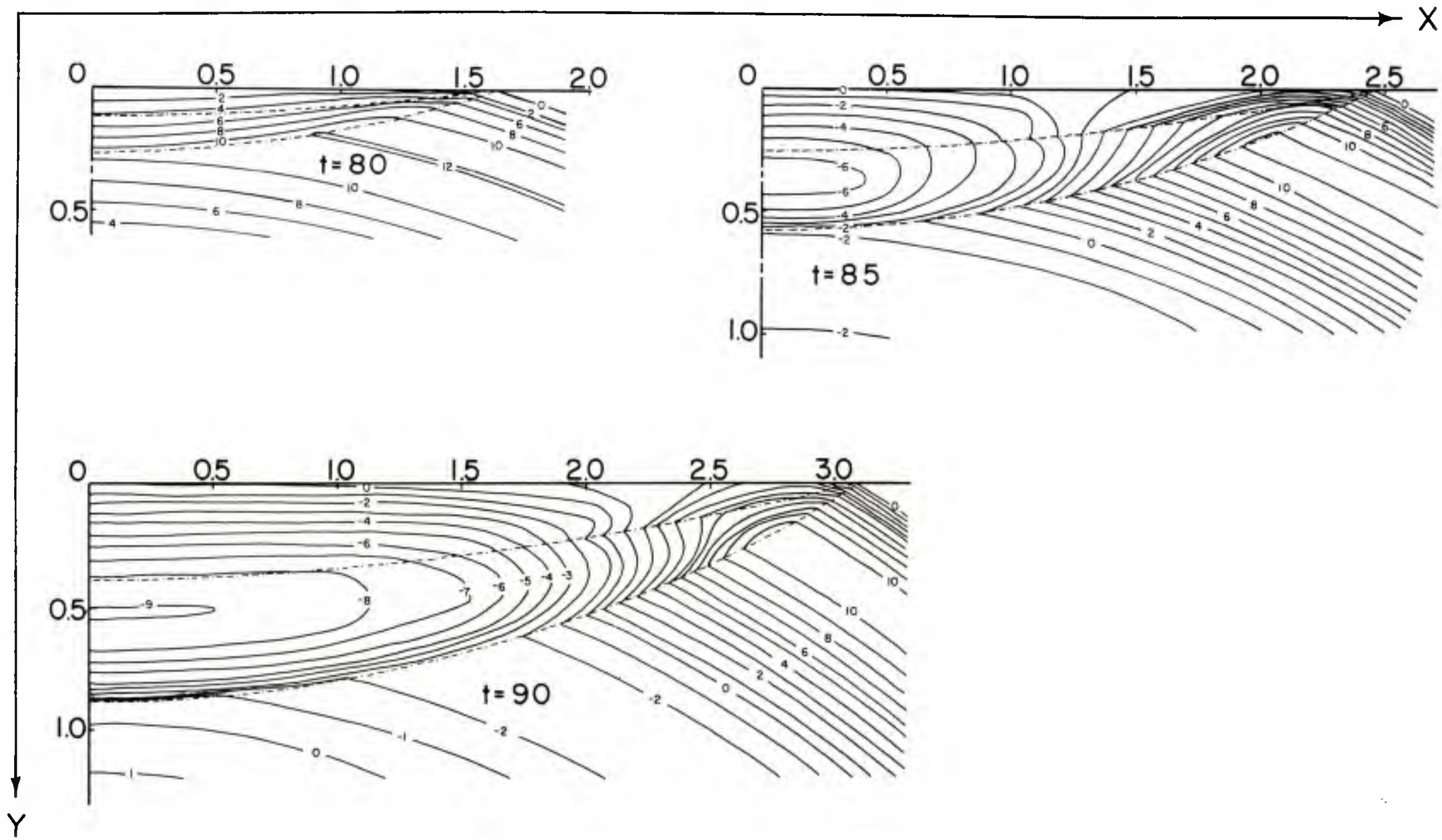

Figure 12. Maximum principal stress (p) for t-values of 80, 85, and 90.

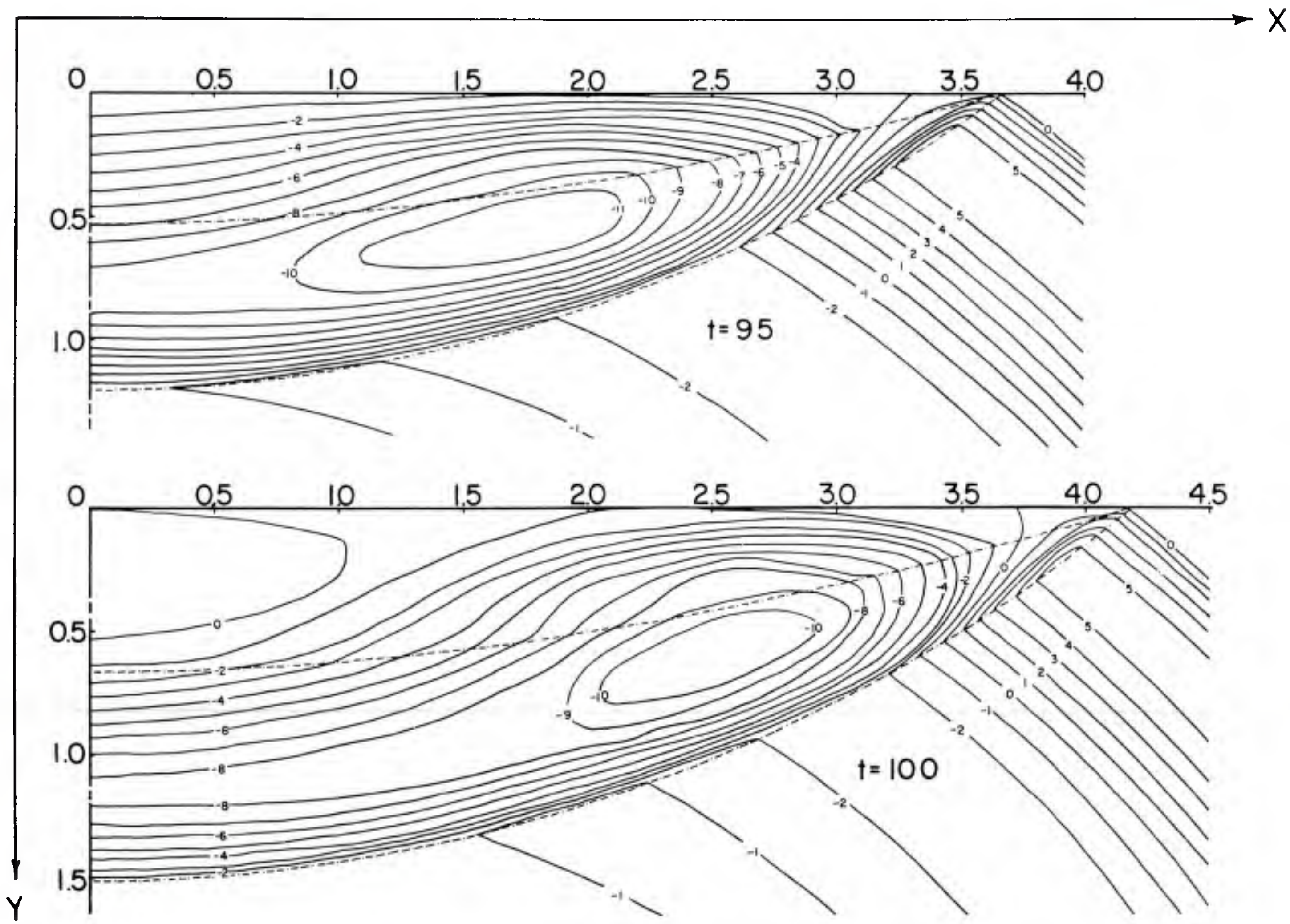

Figure 13. Maximum principal stress (p) for t-values of 95 and 100.

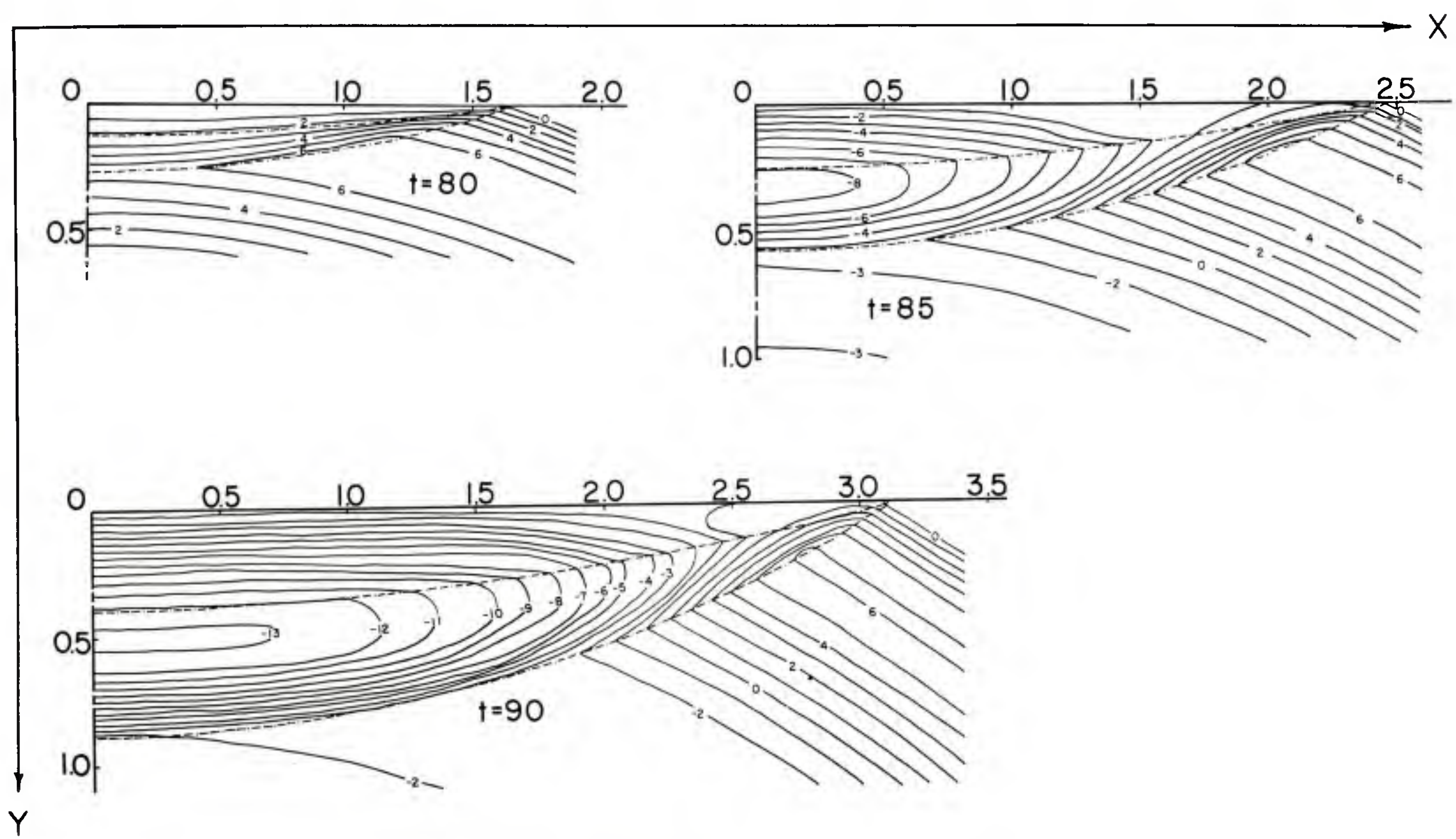

Figure 14. Minimum principal stress (q) for t-values of 80, 85, and 90.

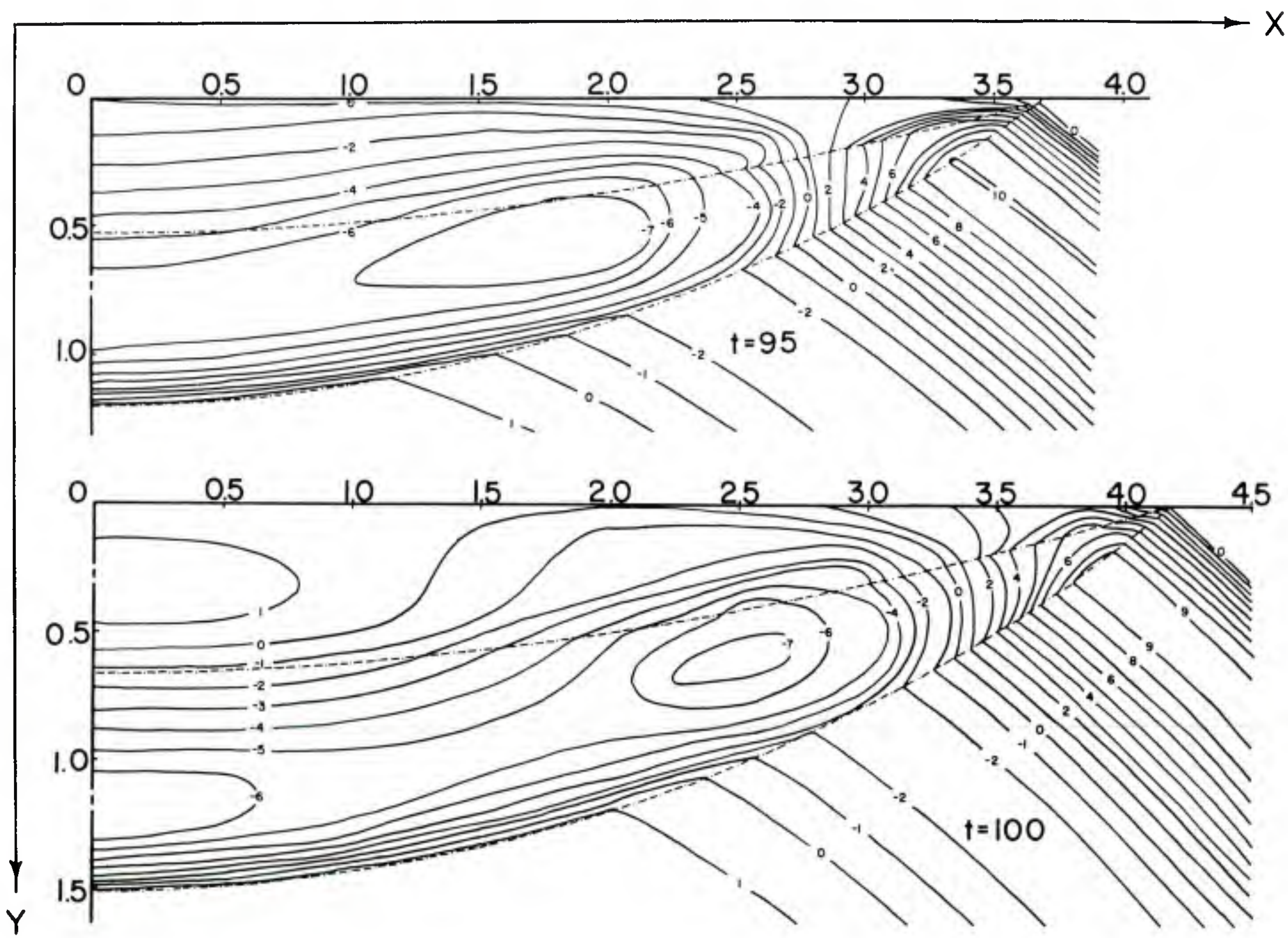

Figure 15. Minimum principal stress (q) for t-values of 95 and 100.

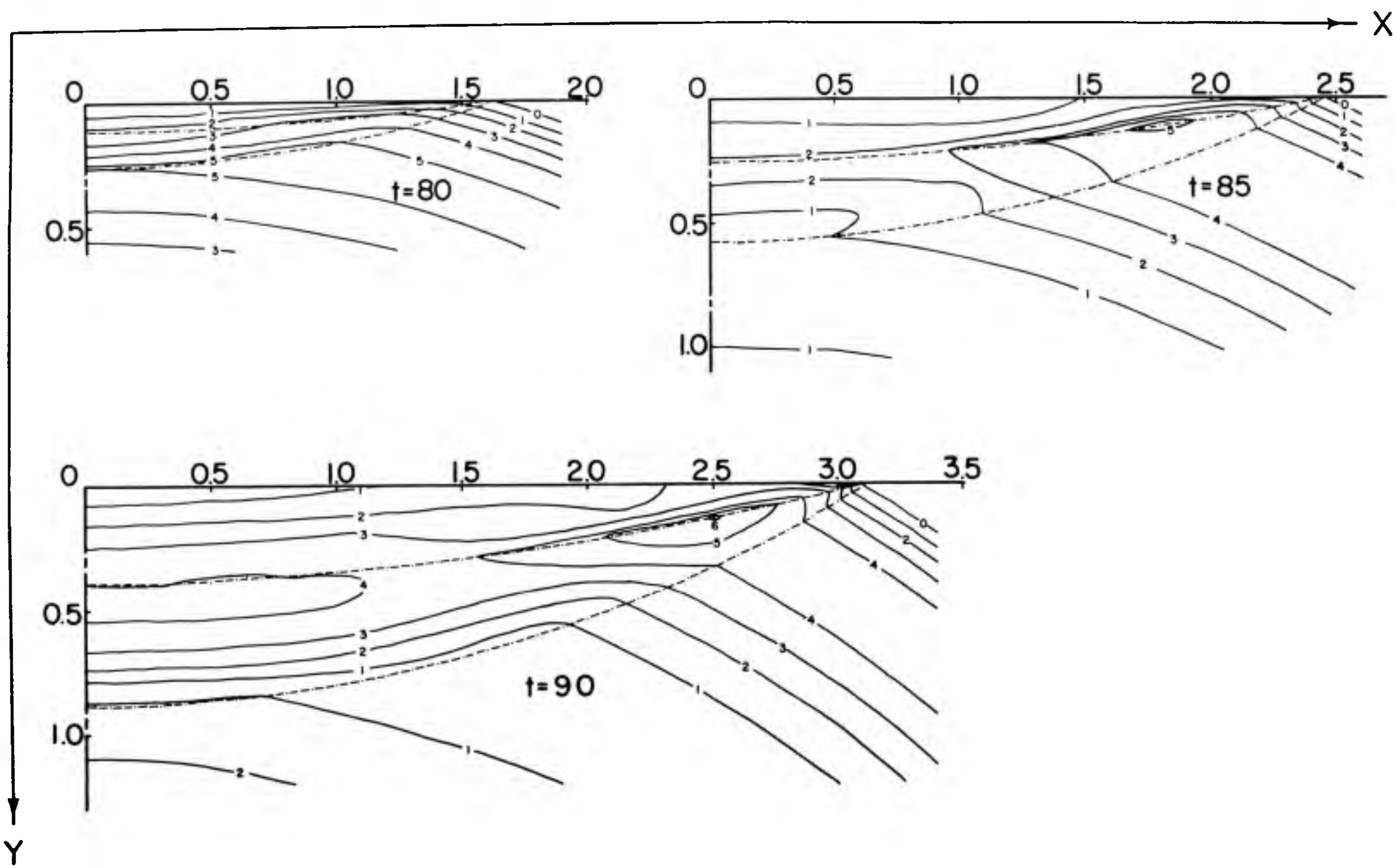

Figure 16. Minimum shear stress (p – q) for t-values of 80, 85, and 90.

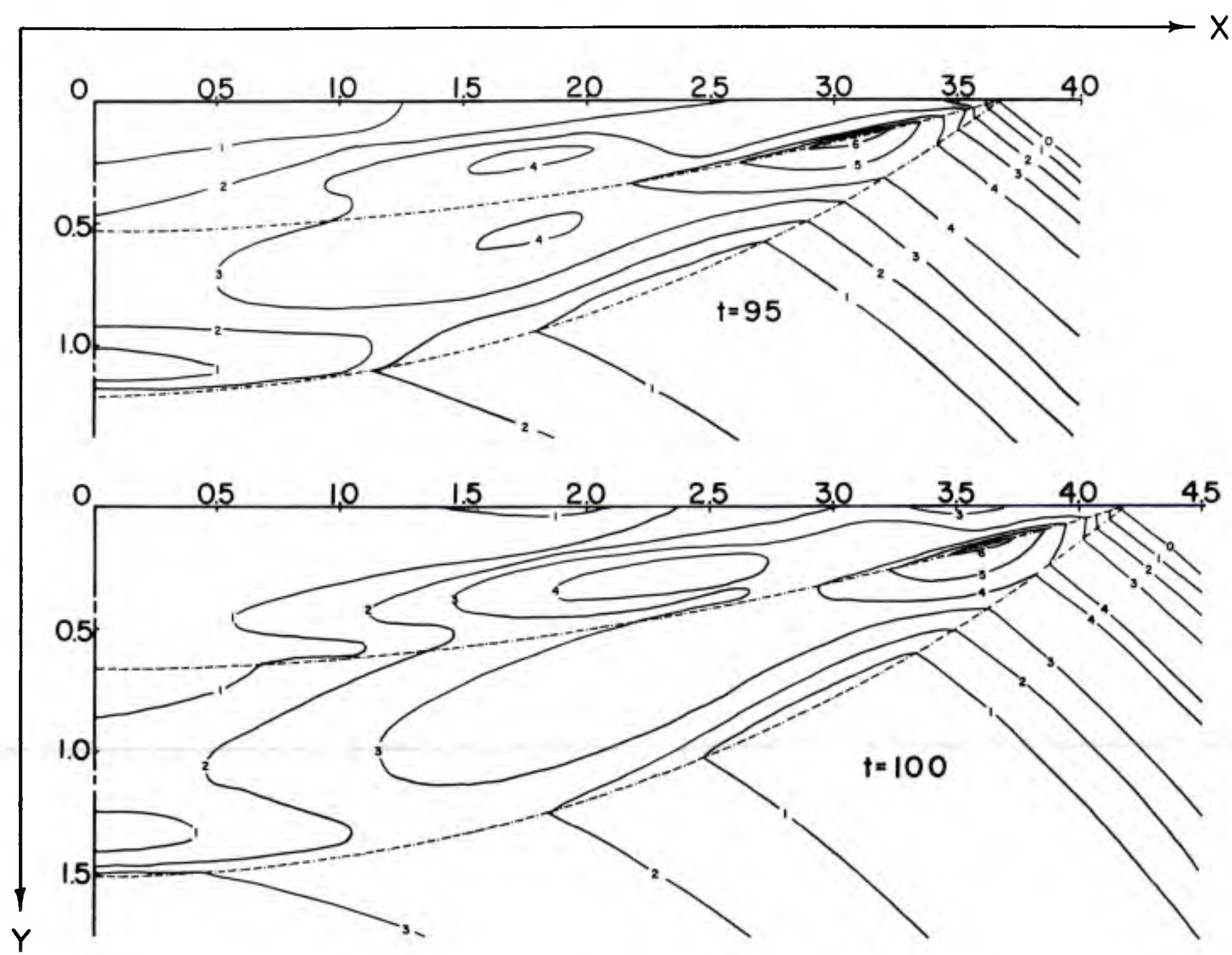

Figure 17. Maximum shear stress (p - q) for t-values of 95 and 100.

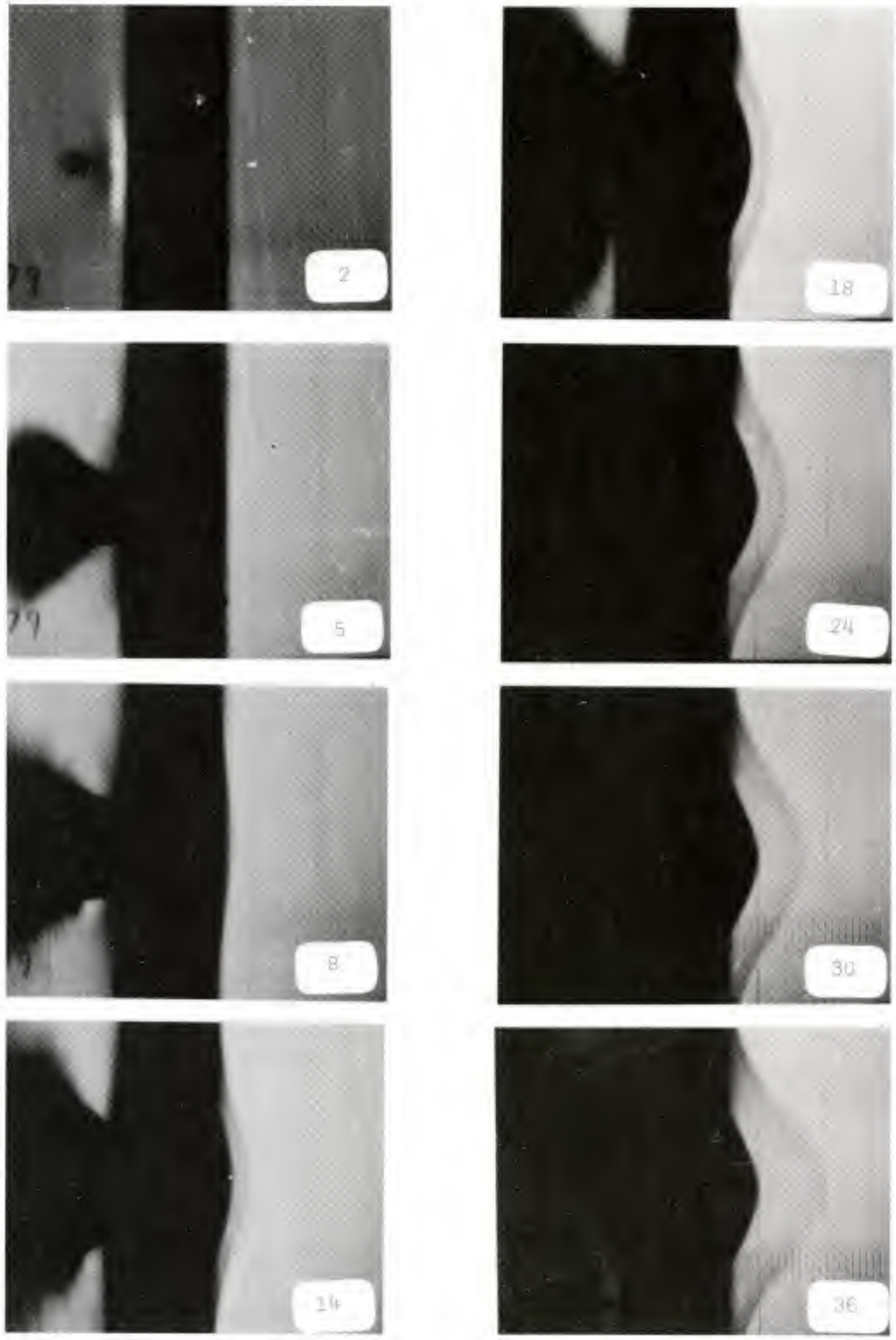

Figure 18. Deformation of rear surface.

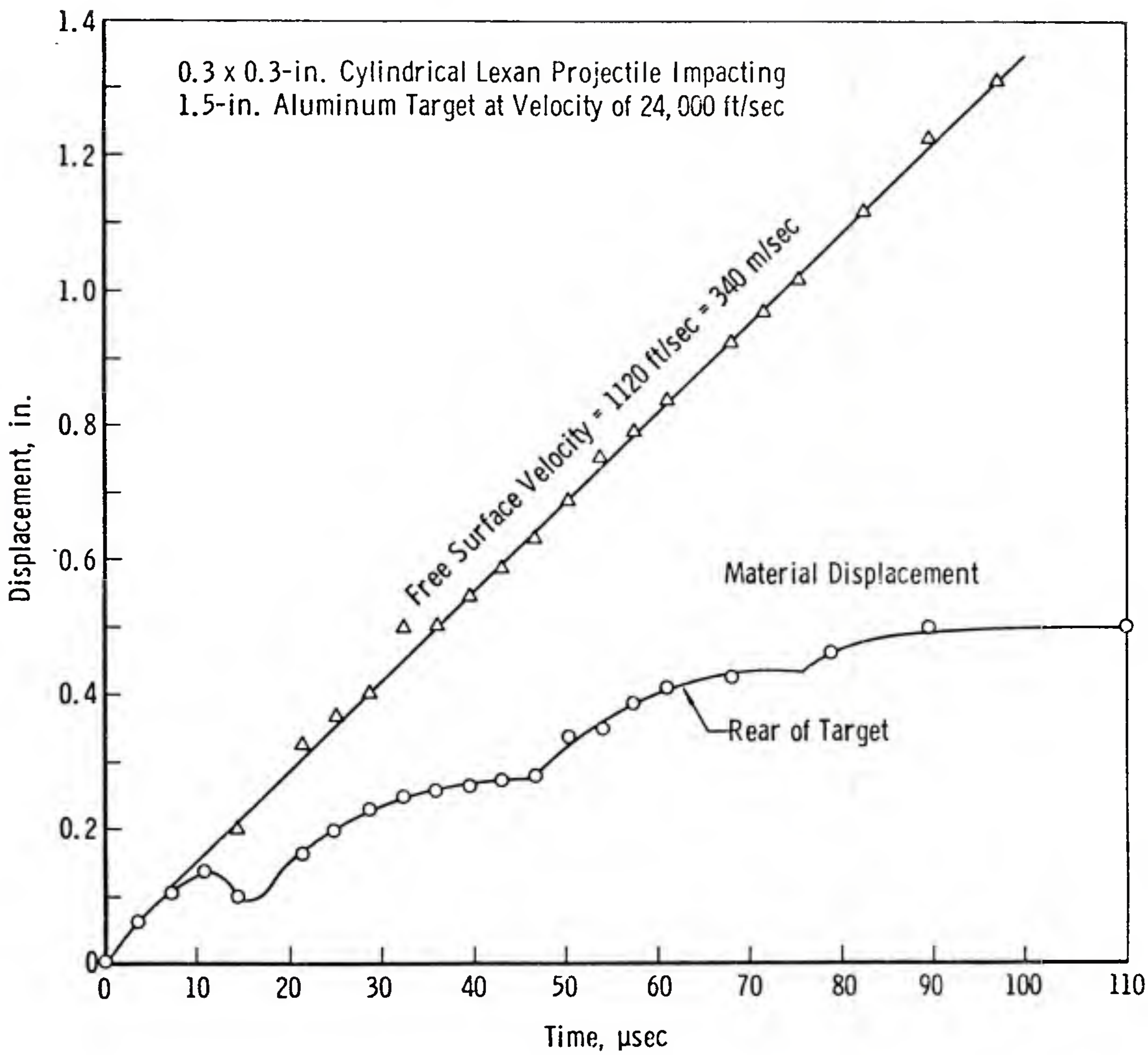

Figure 19. Displacement of rear surface as a function of time.

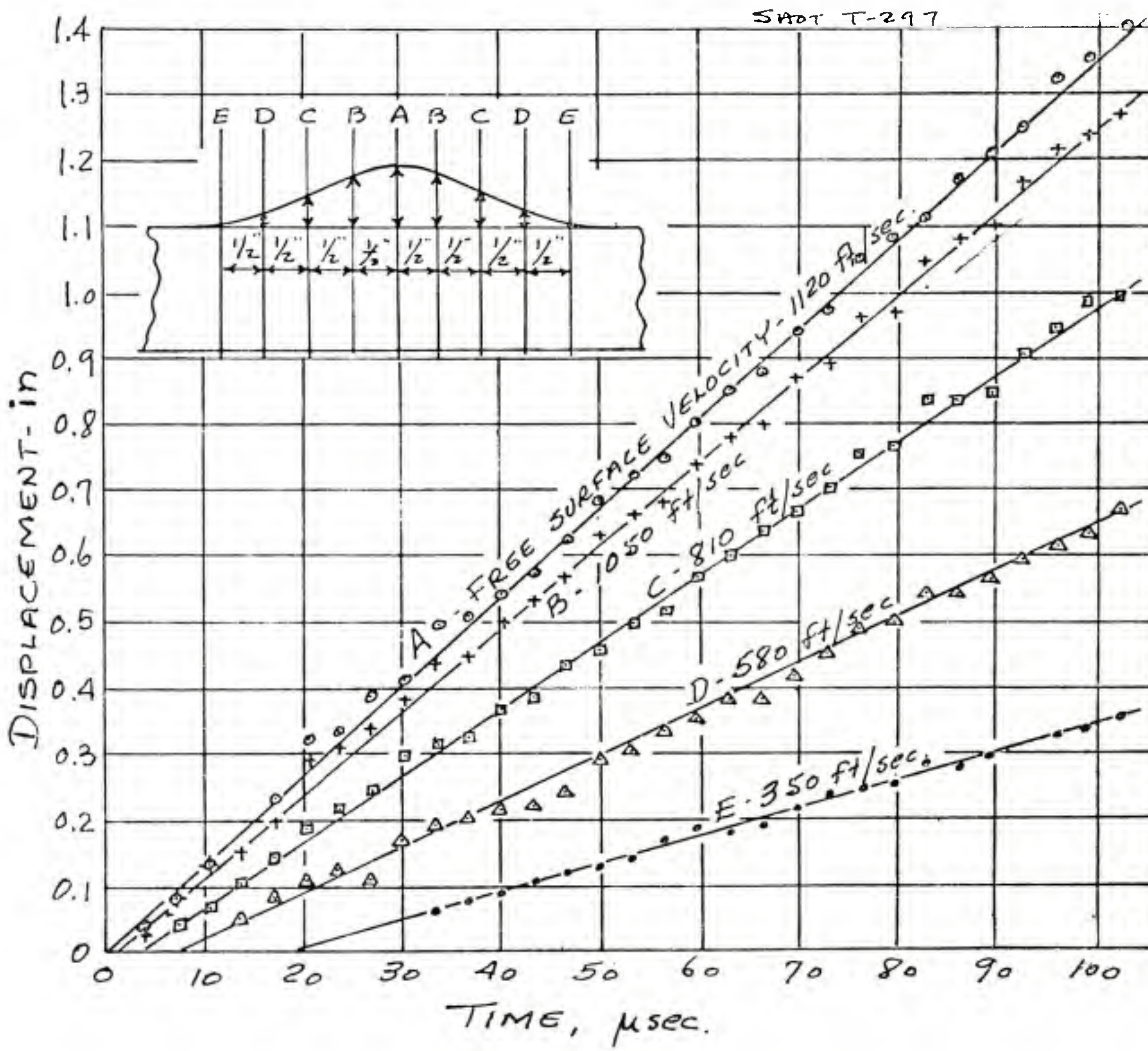

Figure 20. Initial surface velocities at various locations.

Figure 21. Front surface cratering and rear surface fractures.

6. **Conclusion.** It is apparent that spall thickness and velocity depend upon the material properties and upon the pulse profile, or waveform, as well as upon the pulse amplitude. These can be controlled to a large extent by the projectile material and dimensions as well as by its velocity.

The question arises as to the optimum thickness of the spall. If the fracture is near the target surface, the material will be detached very easily, but the kinetic energy of the fragments will be small. A thicker spall would result in greater kinetic energy if it became detached and if a large amount of work was not required to break such a spall loose from the target.

It is obvious that much more work, both theoretical and experimental, needs to be done before the spallation process can be understood to the extent of enabling one to design projectiles that will result in predictable damage.

DISTRIBUTION FOR MERADCOM REPORT 2179

No. Copies	Addressee
	Department of Defense
1	Director, Technical Information Defense Advanced Research Projects Agency 1400 Wilson Blvd Arlington, VA 22209
1	Director Defense Nuclear Agency ATTN: STTL Washington, DC 20305
12	Defense Documentation Center Cameron Station Alexandria, VA 22314
1	Director Defense Nuclear Agency ATTN: Mr. Jim Moulton Washington, DC 20305
1	Director of Defense, Research & Engineering (OSD) ATTN: Mr. J. Persh Washington, DC 20301
1	Director of Defense Research & Engineering (OSD) ATTN: Mr. G. R. Makepeace Washington, DC 20301
3	Director Defense Advanced Research Projects Agency ATTN: Dr. Ernie Blase Dr. Robert Moore Dr. Heilmyer 1400 Wilson Blvd Arlington, VA 22309
	Department of the Army
6	Commander US Army Materiel Development and Readiness Command ATTN: DRCRD-WB DRCRD-T DRCRD-J DRCRD-O DRCRD-G DRCRD-FP 5001 Eisenhower Ave Alexandria, VA 22333
1	Commander, HQ TRADOC ATTN: ATEN-ME Fort Monroe, VA 23651
1	HQDA (DAMA-AOA-M) Washington, DC 20310
1	HQDA (DALO-TS M-P) Washington, DC 20310
1	HQDA (DAEN-RDL) Washington, DC 20314
1	HQDA (DAEN-MCE-D) Washington, DC 20314
1	Commander US Army Missile Research & Development Command ATTN: DRSMI-RR Redstone Arsenal, AL 35809
1	Chief, Engineer Division DCSLOG ATTN: AFKC-LG-E HQ Sixth US Army Presidio of San Francisco, CA 94129
1	Director Army Materials and Mechanics Research Center ATTN: DRXMR-STL Technical Library Watertown, MA 02172
1	US Army Ballistic Research Laboratories Technical Library DRXBR-LB (Bldg 305) Aberdeen Proving Ground, MD 21005
1	Commander Edgewood Arsenal ATTN: SAREA-TS-L Aberdeen Proving Ground, MD 21010
1	Commander US Army Aberdeen Proving Ground ATTN: STEAP-MT-U (GE Branch) Aberdeen Proving Ground, MD 21005

No. Copies	Addressee
1	Director US Army Materiel Systems Analysis Agency ATTN: DRXSY-CM Aberdeen Proving Ground, MD 21005
1	Director US Army Engineer Waterways Experiment Station ATTN: Chief, Library Branch Technical Information Center Vicksburg, MS 39180
1	Commander Picatinny Arsenal ATTN: SARPA-TS-S No. 59 Dover, NJ 07801
1	Commander US Army Troop Support & Aviation Materiel Readiness Command ATTN: DRSTS-KTE 4300 Goodfellow Blvd St Louis, MO 63120
2	Director Petrol & Fld Svc Dept US Army Quartermaster School Fort Lee, VA 23801
1	Commander US Army Electronics Research & Development Command ATTN: DRSEL-GG-TD Fort Monmouth, NJ 07703
1	President US Army Aviation Test Board ATTN: STEBG-PO Fort Rucker, AL 36360
1	US Army Aviation School Library PO Drawer 0 Fort Rucker, AL 36360
1	HQ, 193D Infantry Brigade (CZ) Directorate of Facilities Engineering Fort Amador, Canal Zone
1	Commander Special Forces Detachment (Airborne), Europe APO New York 09050
1	HQ, USAREUR & Seventh Army DCSENGR, ATTN: AEAEN-MO ATTN: Mil Ops Div APO New York 09403
2	Engineer Representative US Army Standardization Group, UK Box 65, FPO New York 09510
1	Commander Rock Island Arsenal ATTN: SARRI-LPL Rock Island, IL 61201
1	Plastics Technical Evaluation Center Picatinny Arsenal, Bldg 176 ATTN: A. M. Anzalone SARPA-FR-M-D Dover, NJ 07801
1	Commander Frankford Arsenal ATTN: Library, K2400, B1 51-2 Philadelphia, PA 19137
1	Learning Resources Center US Army Engineer School Bldg 270 Fort Belvoir, VA 22060
1	President US Army Airborne, Communi- cations & Electronics ATTN: STEBF-ABTD Fort Bragg, NC 28307
1	Commander Headquarters, 39th Engineer Battalion (Cbt) Fort Devens, MA 01433
1	President US Army Armor and Engineer Board ATTN: ATZK-AE-TD-E Fort Knox, KY 40121
1	Commandant US Army Command and General Staff College ATTN: ATSW-RI-L Fort Leavenworth, KS 66027

No. Copies	Addressee
1	Commander 2nd Engineer Group ATTN: S4 APO San Francisco 96301
1	Commander and Director USAFESA ATTN: FESA-RTD Fort Belvoir, VA 22060
1	Dr. Malcolm Curroy ODDR&E The Pentagon Washington, DC
1	Director Army Material Systems Analysis Agency ATTN: M. Smith Aberdeen Proving Ground, MD 21005
3	Commander US Army Armaments Command ATTN: J. A. Brinkman, Tech Dir Dr. Richard Moore W. Wohlford Rock Island Arsenal, IL 61201
1	HQDA (DARD-ARP-E Dr. J. Bryant) Washington, DC 21310
1	Director Ballistics Research Laboratory ATTN: Dr. Robert Eichelberger Tech Dir Aberdeen Proving Ground, MD 21005
1	Clint Frank Ballistics Research Laboratory Aberdeen Proving Ground, MD 21005
1	Director Ballistics Research Laboratory ATTN: Dr. William Gillich Aberdeen Proving Ground, MD 21005
1	Director Ballistics Research Laboratory ATTN: Dr. John Frazier Aberdeen Proving Ground, MD 21005
1	Technical Director MICOM ATTN: Dr. Post Hallowes Dir, Phys. Sci. Directorate Redstone Arsenal, AL 35809
3	Commander Picatinny Arsenal ATTN: Mr. Sidney Jacobson SARPA-AD-D-2 Mr. William Painter Tech Dir J. Pearson Dover, NJ 07801
1	Assistant Secretary of the Army (R&D) ATTN: Dr. K. C. Ernarson Assistant for Research Washington, DC 21310
1	Headquarters Dept of the Army ATTN: Mr. David Hardison Adv for RDA Analysis Rm 3E411 Pentagon, Washington, DC 20310
1	HQDA (DARD-ARZ-B Dr. I. R. Hershner) Washington, DC 20310
1	USA Mobility Equipment Research & Development Command ATTN: DRXFB-VM Mr. Howard E. Horner Fort Belvoir, VA 22060
1	Dr. John C. Hurt USA Research Office P.O. Box 12211 Research Triangle Park, NC 27709
1	US Army ABMDA ATTN: Leonard I. Kopeikin Commonwealth Bldg 1320 Wilson Ave Arlington, VA 22209
1	USA Natick Research & Development Command ATTN: DRXNM-VTF Dr. Roy C. Laible Kansas Street Natick, MA 01760

No. Copies	Addressee
1	HQDA (DARD-ZC Dr. M. E. Lasser) Washington, DC 20310
1	Charles Lehner Advanced Research Projects Agency 1400 Wilson Blvd Arlington, VA 22209
1	Ballistics Research Laboratories ATTN: Dr. Gerry Moss Aberdeen Proving Ground, MD 21005
1	Mr. Cliff McClain Ballistic Missile Defense Agency 1300 Wilson Blvd Arlington, VA 22209
2	Director US Army Mechanics and Materials Research Agency ATTN: J. Mescall Dr. Ed Wright, Assoc Dir Watertown, MA 02172
1	COL Lothrop Mittenthal USA Research Office P.O. Box 12211 Research Triangle Park, NC 27709
1	AMSWE-RDR Dr. Richard Moore Armaments Command Rock Island Arsenal, IL 61201
2	US Army Research Office ATTN: Dr. James Murray Dr. George Mayer Box 12211, Research Triangle Durham, NC 27709
1	Ballistics Research Laboratories ATTN: Paul Netherwood Aberdeen Proving Ground, MD 21003
1	Commander US Army Training and Doctrine Command ATTN: Dr. M. Pastel, ATCD-SI Fort Monroe, VA 23651

No. Copies	Addressee
1	US Army Tank Autom Dev Com ATTN: AMDTA-RK Victor Pagano Warren, MI 48090
1	Dr. Hermann Robl USA Research Office P.O. Box 12211 Research Triangle Park, NC 27709
1	Ballistics Research Laboratory ATTN: Dr. Harry Reed Aberdeen Proving Ground, MD 21005
1	Ballistics Research Laboratories ATTN: Dr. Richard Vitali Aberdeen Proving Ground, MD 21005
1	Director of Defense Research & Engineering ATTN: Mr. R. Thorkildsen Washington, DC 20301
1	Director US Army Materiel Systems Analysis Agency ATTN: AMXSY-D Dr. J. Sperrazza Aberdeen Proving Ground, MD 21005
1	Dr. Edward A. Saibel USA Research Office P.O. Box 12211 Research Triangle Park, NC 27709
1	Dr. Dilip Shah SARRI-LR-4833 Rock Island Arsenal Rock Island, IL 61201
1	HQDA (DARD-DDZ-P Dr. R. B. Watson) Washington, DC 21310
1	Dr. Robert Weigel ARDC Provisional Headquarters DRCSA-RP Building 3002 Picatinny Arsenal Dover, NJ 07801

No. Copies	Addressee
1	COL Wm. Whitaker DARPA 1400 Wilson Blvd Arlington, VA 22209
	MERADCOM
1	Commander Technical Director Assoc Tech Dir/R&D Assoc Tech Dir/Engrg & Acq Assoc Tech Dir/Matl Asmt Assoc Tech Dir/Tech Asmt CIRCULATE
1	Chief, Lab 1000 Chief, Lab 2000 Chief, Lab 3000 Chief, Lab 4000 Chief, Lab 5000 Chief, Lab 6000 Chief, Lab 8000 Chief, Lab 9000 Chief, TARSO CIRCULATE
3	Lab 7000
30	Spec Proj Div (Dr. J. W. Bond)
3	Tech Reports Ofc
3	Security Ofc
2	Tech Library
1	Requirements & Programs Ofc
1	Information Ofc
1	Legal Ofc
	Department of the Navy
1	Director, Physics Program (421) Office of Naval Research Arlington, VA 22217
1	Director Naval Research Laboratory ATTN: Code 2627 Washington, DC 20375

No. Copies	Addressee
1	Commander, Naval Facilities Engineering Command Department of the Navy ATTN: Code 032-A 200 Stovall St Alexandria, VA 22332
1	US Naval Oceanographic Office Library (Code 1600) Washington, DC 20373
1	Officer-in-Charge (Code L31) Civil Engineering Laboratory Naval Construction Battalion Center Port Hueneme, CA 93043
1	Director Earth Physics Program Code 463 Office of Naval Research Arlington, VA 22217
3	Commander ATTN: Walter Atkins Mario Persechino Tech Director Naval Research Laboratories Washington, DC 20332
2	Commander US Naval Weapons Center ATTN: Mr. Backman Dr. John Pearson China Lake, CA 93555
1	Commander Naval Surface Weapons Center ATTN: Dr. Arnold Siegel White Oaks, MD 20910
1	Dr. Jack Goeller Naval Surface Weapons Center/WOL Code 322 Silver Spring, MD 20910
1	Commander US Naval Surface Weapons Center ATTN: Dr. R. E. Wilson Silver Spring, MD 10910

No. Copies	Addressee
	Department of the Air Force
1	HQ USAF/RDPS (Mr. Allan Eaffy) Washington, DC 20330
1	Mr. William J. Engle Chief, Utilities Branch HQ USAF/PREEU Washington, DC 20332
1	AFSC/INJ Andrews AFB, MD 20334
1	AFCEC/XR/21 Tyndall AFB, FL 32401
1	HQ USAF/PREES ATTN: Mr. Edwin B. Mixon Bolling AFB-Bldg 626 Washington, DC 20332
1	AFAPL/SFL Wright-Patterson AFB, OH 45433
1	Department of Transportation Library, FOB 10A, TAD-494.6 800 Independence Ave., SW Washington, DC 20591
1	AFATL (DLB, Dr. B. A. Kulp) Eglin AFB, FL 32542
1	MG Jasper A. Welch, Jr. Asst C/S, Studies & Analyses HQ USAF/SA Pentagon Washington, DC 20330
	Others
1	Professor Raymond R. Fox School of Engineering and Applied Science The George Washington University Washington, DC 20052

No. Copies	Addressee
1	Professor Jan D. Achenbach Department of Civil Engineering Technological Institute Northwestern University Evanston, IL 60201
1	Professor Carl Altstetter 302 MMB Department of Metallurgy & Mining Engineering College of Engineering University of Illinois at Urbana-Champaign Urbana, IL 61801
1	Professor A. S. Argon Room 1-312 Massachusetts Institute of Technology Cambridge, MA 02139
1	Mr. Charles A. Anderson President Stanford Research Institute Menlo Park, CA 94025
2	Battelle Columbus Laboratories ATTN: Dr. Dale Trott Stan Goddard 505 King Ave Columbus, OH 43201
2	Aerospace Corp ATTN: Mr. Thor Bergstralh Dr. Sidney Kash El Sugundo, CA 90245
1	Dr. R. S. Carbonara Battelle Columbus Laboratories - Durham, Office Durham, NC 27707
1	Professor R. J. Clifton Division of Engineering Brown University Providence, RI 02912
1	Dr. D. R. Curran Stanford Research Institute Menlo Park, CA 94025
1	Prof Keith Bruazhner Physics Dept Univ of Calif at San Diego San Diego, CA 92109

No. Copies	Addressee
1	Dr. John Batch Director Battelle Columbus Laboratories 505 King Avenue Columbus, OH 43201
1	Professor Ian M. Fyfe FS-10 Department of Aeronautics & Astronautics University of Washington Seattle, WA 98195
1	Steven Gill ARTEC Associates, Mc 26046 Eden Landing Road Hayward, CA 94545
1	Charles S. Godfrey Physics International Co 2700 Merced Street San Leandro, CA 94577
1	Professor J. Duffy Division of Engineering Brown University Providence, RI 02912
1	Professor Victor A. Greenhut College of Engineering Rutgers University New Brunswick, NJ 08903
1	Dr. David W. Hoeppner University of Missouri-Columbia College of Engineering–Rm 2007 Columbia, MO 65201
1	Prof Ray Kinslow Box 5002 Tennessee Technological University Cookeville, TN 38501
1	Professor George Krauss Department of Metallurgical Engineering Colorado School of Mines Golden, CO 80401
1	Professor Campbell Laird Department of Metallurgy & Materials Sciences University of Pennsylvania Bldg K1 Philadelphia, PA 19174

No. Copies	Addressee
1	Dr. James Lankford Southwest Research Institute P.O. Drawer 28510 San Antonio, TX 78284
1	Dr. W. C. Lau Room 1-312 Massachusetts Institute of Technology Cambridge, MA 02139
1	Professor J. C. M. Li Department of Mechanical & Aerospace Sciences University of Rochester Rochester, NY 14627
1	Professor Hao-Wen Liu 409 Link Hall Syracuse University Syracuse, NY 13210
1	Professor L. E. Malvern Engineering Sciences Department 231 Aero Bldg University of Florida Gainesville, FL 32611
1	Professor Donald E. Mikkola Department of Metallurgical Engineering Michigan Technological University Houghton, MI 49931
1	Professor Oscar Orringer Department of Aeronautics & Astronautics Massachusetts Institute of Technology Cambridge, MA 02139
1	Dr. A. Narath Vice President, Research Organization 5000 Sandia Laboratories Albuquerque, NM 87115
1	Professor Arthur Paskin Queens College of the City University of New York Flushing, NY 11367

No. Copies	Addressee
1	Professor J. N. Reddy The University of Oklahoma 865 Asp Avenue Room 200 Norman, OK 73069
1	Professor Harry C. Rogers Department of Materials Engineering Drexel University Philadelphia, PA 19104
2	R&D Associates ATTN: Dr. Albert Latter Dr. Marvin Schafer P.O. Box 3580 525 Wilshire Blvd Santa Monica, CA 90403
1	Professor Martin Sommerfield University of Princeton Princeton, NJ 08540
1	Paul Tamarkin Rand Corporation Santa Monica, CA 90406
1	Professor Dale F. Stein Department of Metallurgical Engineering Michigan Technological University Houghton, MI 49931
1	Professor Robert Stilker Department of Aeronautics & Astronautics Massachusetts Institute of Technology Cambridge, MA 02139
1	Professor T. C. T. Ting Department of Materials Engineering University of Illinois at Chicago Circle Chicago, IL 60680
1	K. D. Seifert Physics International Co 2700 Merced Street San Leandro, CA 94577
1	Professor Volker Weiss Conference Secretariat, ICM-II American Society for Metals Metals Park, OK 44073

No. Copies	Addressee
3	Lawrence Livermore Laboratory ATTN: Tech Director Mark Wilkins Dr. Edward Teller Livermore, CA 94550
1	Professor John Williams School of Engineering The University of Connecticut Storrs, CT 06268
1	Professor Kenneth Watson Physics Dept University of Calif Berkely CA 94720
1	Dr. Donald Shockey Stanford Research Institute Menlo Park, CA 94025
1	Dr. D. R. Curran Stanford Research Institute Menlo Park, CA 94025

1 2 69,707—AG—Ft Belvoir